Chemical Engineering Journal xxx (xxxx) xxxx

Contents lists available at ScienceDirect

Chemical Engineering Journal

journal homepage: www.elsevier.com/locate/cej

Surface functionalization of few-layer black phosphorene and its flame retardancy in epoxy resin

Zhencai Qu[a,b], Kun Wu[a,*], Enxiang Jiao[a,b], Weilong Chen[a,b], Zhuorong Hu[a,b], Changan Xu[a,b], Jun Shi[a], Shan Wang[a,b], Zhiyou Tan[a,b]

[a] Key Laboratory of Cellulose and Lignocellulosics Chemistry, Guangzhou Institute of Chemistry, Chinese Academy of Sciences, Guangzhou 510650, PR China
[b] University of Chinese Academy of Sciences, Beijing 100039, PR China

HIGHLIGHTS

- Few-layer black phosphorene was successfully functionalized by MF resin.
- Significantly enhanced flame retardant efficiency was achieved.
- Scavenging free radicals and catalyzing char formation were the main mechanism.

ARTICLE INFO

Keywords:
Black phosphorene
Flame retardant
Density functional theory
Mechanism
Nanocomposites

ABSTRACT

Similar to graphene, single or few-layer of black phosphorus (BP) are promising for its high thermal stability and unique characteristic dimension effects. However, the agglomeration problem of BP nanosheets in polymer matrix renders great difficulty toward its application. Herein, Melamine-formaldehyde (MF) is conducted to functionalize black phosphorus (BP) nanosheets. Based on density functional theory (DFT) calculations, the adsorption energy is −0.63 eV, which suggests there exists a strong mutual adsorption between BP nanosheets and MF. The functionalized BP (BP@MF) is introduced into epoxy resin (EP) to evaluate its thermal stability and flame retardant properties. BP@MF can successfully solve the aggregation phenomenon due to the improved dispersibility of BP in EP matrix. With the incorporation of 1.2 wt% BP@MF into EP matrix, the char yield is dramatically improved by 70.9%, which is attributed to the outstanding thermal stability and the catalytic charring effect of BP@MF. EP/BP@MF nanocomposites can pass the UL-94V-0 rating, and the limiting oxygen index value increases by 25.9%. The peak of heat release rate is reduced by 43.3% and the fire growth rate decreases by 41.2%, which is ascribed to the inhibition of heat transfer and isolation of oxygen by BP@MF. Meanwhile, BP@MF reveals an extremely high flame retardant efficiency by a small addition amount. Below 400 °C, MF sublimates to absorb heat and BP@MF promotes the formation of an expanded carbon layer. Above 400 °C, BP may scavenge free radicals and catalyze char formation. As one new nanofiller of 2D materials, BP has great potential to fabricate high-performance nanocomposites.

1. Introduction

Black phosphorus (BP), the most thermodynamically stable and the least reactive allotrope of phosphorus has an orthogonal puckered layer, which is formed by P atoms covalently bonded to other three P atoms [1,2]. The single- or few-layer BP exfoliated from a black phosphorus crystal is identified “phosphorene” [3]. Now phosphorene become a novel two-dimensional material, which is similar to graphene, has attracted a great attention in recent years [4]. Compared to conventional 2D materials such as graphene [5], graphene derivatives [6], transition metal dichalcogenides [7], hexagonal boron nitride [8], graphitic carbon nitride [9] and MXenes [10]. BP has controllable band gaps (0.3–2 eV from bulk to single layer) [11], broad ultraviolet absorption range and catalytic activity [12], and is widely used in sensors, super capacitors, electrochemical and biomedical fields [13]. Meanwhile, by right of its unique characteristic size effect, good mechanical properties and high thermal stability, the single or few-layer BP is expected to be a new nanofiller for the manufacture of high-performance polymer nanocomposites [14].

Since the first successful exfoliation of phosphorene by scotch-tape

* Corresponding author.
E-mail address: wukun@gic.ac.cn (K. Wu).

https://doi.org/10.1016/j.cej.2019.122991
Received 12 July 2019; Received in revised form 5 September 2019; Accepted 27 September 2019
1385-8947/ © 2019 Elsevier B.V. All rights reserved.

micro-cleavage method in 2014, the preparation of single or few-layer of BP has become a research hotspot for the application of phosphorene [14,15]. So far, the preparation of black phosphorus crystals mainly includes ball milling method and red phosphorus mineralization method. Due to the harsh conditions required for ball milling method, the yield of black phosphorus is very low. Currently, the laboratory mainly uses chemical vapor transport method to convert red phosphorus into black phosphorus. The red phosphorus, Sn, and SnI_4 are sealed in a quartz tube and heated to 650 °C at a heating rate of 1.35 °C min^{-1} in a vacuum tube furnace, then keep the temperature at 650 °C for 5 h, and cool it to 500 °C at a cooling rate of 0.33 °C min^{-1}. Finally, the target product is separated from the residual mineralizer by toluene refluxing to obtain black phosphorus crystal. Unlike its 3D parent, the top-down approach is extensively used to fabricate phosphorene through various exfoliation strategies, such as mechanical exfoliation [16,17], ball milling [12,16], microwave exfoliation [18], liquid exfoliation in different solvents [19]. The mechanical fabrication can obtain high quality phosphorene, but the efficiency and yield are very low, and mass production cannot be achieved [3,20]. Depending on ball milling method, the few-layer of black phosphorene can be obtained with a small size but the purity is not high [21]. Furthermore, liquid exfoliation has the advantages of simple operation, low cost, high production and good performance, and has become one of the most commonly used methods for the preparation of phosphorene. For instance, N-methyl-2-pyrrolidone [19], dimethylformamide [22], N-cyclohexyl-2-pyrrolidone [17] and isopropanol [23] are employed to exfoliate the BP nanosheets with the assistance of sonication. These methods can prepare few-layer of BP with large size and high quality.

However, the surface of the phosphorene contains a pair of lone pairs of electrons, which are easy to react with oxygen and are highly susceptible to degradation under the action of water. This problem severely restricts the application of phosphorene. Many researchers have done many studies on the surface modification and functionalization of phosphorene and have made some progress. Zhao [24] synthesized a titanium sulfonate ligand to modify black phosphorene, the BP after surface coordination showed excellent stability to the air and water during a long period of time. Zhang [25] reported that negatively charged BP fabricated via lithium ion intercalation indicated much higher reactivity to diazonium modification. The diazonium functionalized BP exhibited high stability to the ambient condition for more than 200 days. Hu [26] demonstrated carbon free radicals from azodiisobutyronitrile (AIBN) molecules could be used to covalently functionalize black phosphorus nanoflakes (BPNFs), the BPNFs after successful modification (BPNFs-AIBN) had good stability and optical properties. Gonzalo Abelln [27] offered a new method for noncovalent functionalization of black phosphorus (BP) with electron-withdrawing 7,7,8,8-tetra-cyano-p-quinodimethane (TCNQ), the noncovalent modification of BP had considerable stabilization against oxygen degradation. Wu [28] prepared lanthanide-coordinated black phosphorus through lanthanide (Ln) sulfonate complexes, the LnL_3@BP manifested excellent stability and other Ln (Tb, Eu and Nd) coordinated BP showed fluorescence spanning to near-infrared regions. However, these studies have a positive effect on the air stability of phosphorene, but there exists some problems such as complicated operation and high cost, and the effect of functionalization on the application of phosphorene is neglected. Hence, it is of great practical significance to improve the practical application of phosphorene by means of functionalization.

As is well known, red phosphorus (RP) and phosphorus-containing compounds are commonly used as flame retardants, but there are problems including the large amount addition and the poor compatibility with the resin. Compared to RP, black phosphorus is a two-dimensional material with greater specific surface area and size effects. It can be converted from red phosphorus under high temperature and high pressure conditions and thus has higher stability. BP has higher thermal stability and more unique layered structure that can inhibit heat transfer and insulate oxygen during combustion. Therefore, it is very important to study the low amount addition of phosphorene to obtain good dispersibility and high flame retardancy efficiency. Ren [29] studied the flame retardancy of black phosphorene-waterborne polyurethane (BPWPU) composite polymer, when the addition of black phosphorene was 0.2 wt%, the limiting oxygen index (LOI) of BPWPU increased by 2.6%, the heat flow decreased by 34.7% and the peak heat release rate (PHRR) decreased by 10.3%. Ren [4] prepared the black phosphorene/graphene (BP/G) composites through the high-pressure nano-homogenizer machine and then incorporated the BP/G into waterborne polyurethane (WPU) to fabricate a flame retardant composites, when the additive amount was 3.55 wt%, the PHRR and the total heat release (THRR) decreased by 48.18% and 38.63%, respectively. However, the method of direct addition of BP or BP/G ignored its poor compatibility with resins, which led to a serious agglomeration in the resin. Qiu [30] used an electrochemical strategy to fabricate cobaltous phytate functionalized BP nanosheets (BP-EC-Exf) and introduced the BP-EC-Exf into polyurethane acrylate (PUA) to prepare PUA/BP-EC flame retardant nanocomposites, when the addition of BP-EC-Exf was 3.0 wt%, the PHRR reduced by 44.5% and the THR decreased by 34.5%. Nevertheless, the number of BP layers stripped by electrochemical method was very thick, so it was unable to maximize the flame retardant effect of BP. Qiu [31] incorporated polyphosphazene-functionalized BP into epoxy resin to study the flame retardant property, when the introduction of BP-PZN was 2.0 wt%, the PHRR decreased by 59.4% and the THRR reduced by 63.6%. The BP-PZN could significantly improve the dispersibility of the phosphorene, and exhibited its excellent flame retardancy. However, HCCP, one of the raw materials, contained chlorine element, which was easy to generate harmful gases during combustion and caused damage to the environment.

MF resin has good biocompatibility, chemical stability and abundant $–NH_2$ groups. Previous studies have demonstrated that graphene quantum dots [32], graphite nanoflakes [33], fluorescent dye [34] and 3D interconnected boron nitride nanosheets [35] could be successfully functionalized by MF resin to improve their dispersibility in resins. In this work, MF resin was employed to modify BP to improve the compatibility of the BP into the resin and its flame retardant efficiency. We developed a facile one-pot method to functionalize BP by MF resin and defined the product as BP@MF, fabricating an inorganic-organic nanofiller for polymer resin (Fig. 1). The resultant BP@MF was then incorporated into epoxy resin to investigate the thermal stability and flame retardant properties. This work expects to achieve excellent flame retardant efficiency with very small addition amount in order to solve the problem of large amount and high cost of traditional flame retardant. Such functionalized strategy is beneficial to enhance the application of black phosphorene and open up new prospects for the fabrication of high-performance nanocomposites.

2. Experimental

2.1. Materials

Black phosphorus crystal (99.998%) was purchased from Zhongke Experimental Materials (China) and preserved in an inert atmosphere. Melamine (99.5%) was provided by Tianjing Kemiou Chemical Reagent Co. Ltd (China). N-methyl-2-pyrrolidone (NMP) (99.0%) and formaldehyde (37%) were purchased from Tianjin Fucheng Chemical Reagents Factory (China). 4,4-Diaminodiphenylmethane (DDM) (99%) was obtained from Aladdin Industrial Corporation (China). EP (DGEBA, E-51) was supplied by Nantong Xingchen Synthetic Materials Co., Ltd. (China). Sodium carbonate (99.8%), acetone (99.5%) and ethanol (99.7%) were purchased from Guangzhou Chemical Reagents Factory (China).

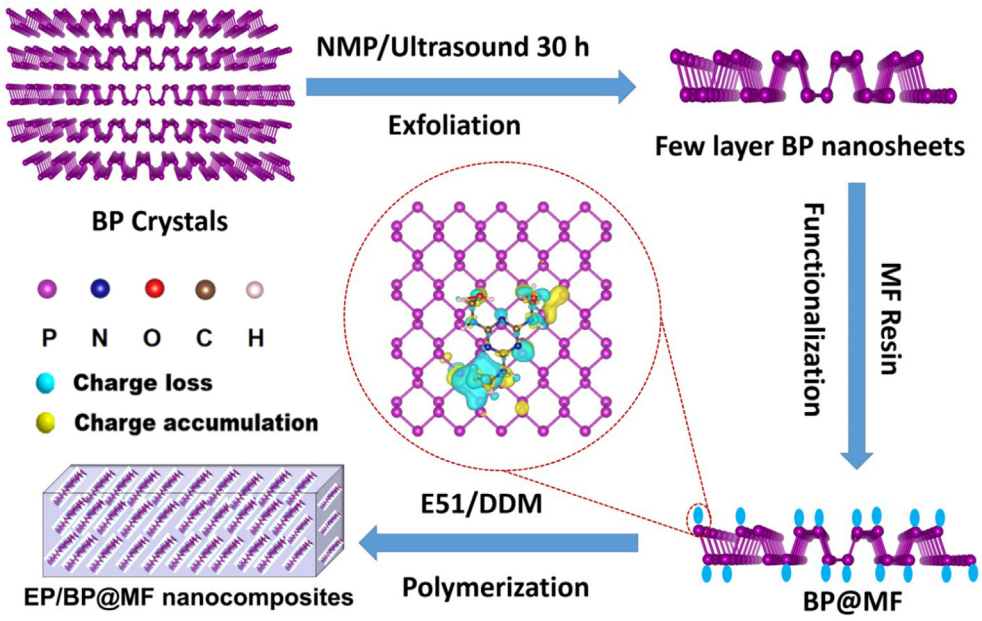

Fig. 1. The preparation process of BP@MF nanofiller and EP/BP@MF nanocomposites.

2.2. Synthesis

2.2.1. Preparation of BP

The black phosphorene was fabricated through a liquid exfoliation method. Black phosphorus crystal (200 mg) was first dispersed in 400 mL of N-methyl-2-pyrrolidone (NMP) with the assistance of ultrasonic cell pulverizer for 60 min, the ultrasonic cell pulverizer worked for 4 s at an interval of 6 s with the power of 650 W. The coarse dispersions were then sonicated in an ice bath (325 W) for 30 h. After that, the BP suspensions were centrifuged at 3000 rpm for 30 min to remove the un-exfoliated BP crystal. Then, the supernatant solutions were further centrifuged at 10,000 rpm for one hour. The collected sediment was washed with ethanol for three times to remove the NMP, and finally dried in a flask under vacuum. The sample was preserved in an inert atmosphere before use, named as black phosphorene (BP).

2.2.2. Synthesis of BP@MF

Synthesis of melamine–formaldehyde (MF) pre-polymer: Melamine (2.0 g) was dispersed in 30.0 mL of distilled water in a flask. Formaldehyde (3.6 mL) was dropped into the solutions at a speed of 2–3 drops per second. The reaction process was continued at 80 °C for 30 min with mechanical stirring (300 rpm) when the PH was maintained at 8–9 with sodium carbonate solution. Then the MF pre-polymer was prepared. Functionalization of BP with MF: BP nanosheets (100 mg) was dispersed in NMP (200 mL), sonicated for 30 min, and then added into half of the prepared MF pre-polymer. The mixture was stirred at 300 rpm under 80 °C for 5 h in nitrogen atmosphere. Finally, the suspension of the mixture was centrifuged at 10,000 rpm for 1 h and washed with ethanol (10 mL × 3), and then dried under vacuum at 120 °C. The resultant product was named BP@MF.

2.2.3. Preparation of EP/BP@MF nanocomposites

Preparation process of EP nanocomposites with the addition of 0.3 wt% BP@MF: 0.15 g of BP@MF and 9.97 g of DDM were dispersed in 20 mL of acetone. Then the mixture was stirred by a magnetic stirrer for 10 min. After that, 39.88 g of epoxy resin (E51) was poured into the mixed system with mechanical stirring (300 rpm) for 30 min. Subsequently, the whole system was placed in a vacuum to remove the acetone with the temperature of 60 °C for 2 h. Finally, the resin mixture was cured in a mold with the procedures of 100 °C/2h, 150 °C/2h, respectively. When the sample was cooled to the room temperature, the resultant nanocomposites was called EP/BP@MF 0.3. A similar procedure was also used for pure EP, EP/BP (1.2 wt%) and the amount (0.6 wt%, 0.9 wt%, and 1.2 wt%) of BP@MF.

2.3. Characterization

Scanning electron microscopy (SEM, Hitachi S3400N) was employed to observe the microstructures of BP and the char residues as well as the fracture surface of EP/BP@MF nanocomposites. Atomic force microscopy (AFM, Dimension Icon) was conducted to reflect the thickness and average size of BP. Transmission electron microscopy (TEM, JEM-1230) was performed to study the morphology of BP and BP@MF. X-ray diffraction (XRD, Rigaku D/MAX-1200) were recorded with Cu Ka radiation (λ = 0.154 nm), in the 2θ range of 1–80°. Fourier transform infrared spectra (FTIR, Bruker TENSOR 27 FTIR) was collected with KBr pellets to test solid samples. Laser Raman spectroscopy was employed through a Renishaw invia Raman spectrometer with excitation at 530 nm from an argon laser to observe the structure of BP@MF and the char layer of EP composites. X-Ray photoelectron spectroscopy (XPS) was utilized by a Thermo Fisher Scientific K-Alpha electron spectrometer. The excitation source of the instrument was an Al K alpha at 1486.8 eV. Thermogravimetric analysis (TGA) was carried out on NETZSCH TG 209F3 thermo-analyzer instrument in nitrogen atmosphere, at a continuous heating rate of 10 °C min^{-1} from 30 °C to 1000 °C. Dynamic mechanical analysis (DMA) was employed to test the dynamic mechanical properties of EP/BP@MF, all the samples were heated from room temperature to 250 °C with a linear heating rate of 5 °C min^{-1}, and the frequency was 1 Hz for the tensile configuration. Optical microscope was conducted to record the dispersity of BP and BP@MF in EP resin, rapid slice was used to prepare samples. A microscale combustion calorimeter was employed to test the heat release rate by a mold of MCC-2 (GOVMARK). About 5 mg of sample was heated at the rate of 1 °C s^{-1}. The carrier gases consist of two gas, N_2 of 80 mL min^{-1} and O_2 of 20 mL min^{-1}, respectively. Thermogravimetric analysis/infrared spectra (TG-IR) was employed with a NETZSCH TG 209F1 thermo-analyzer instrument combined with a Nicolet IS50 spectrometer.

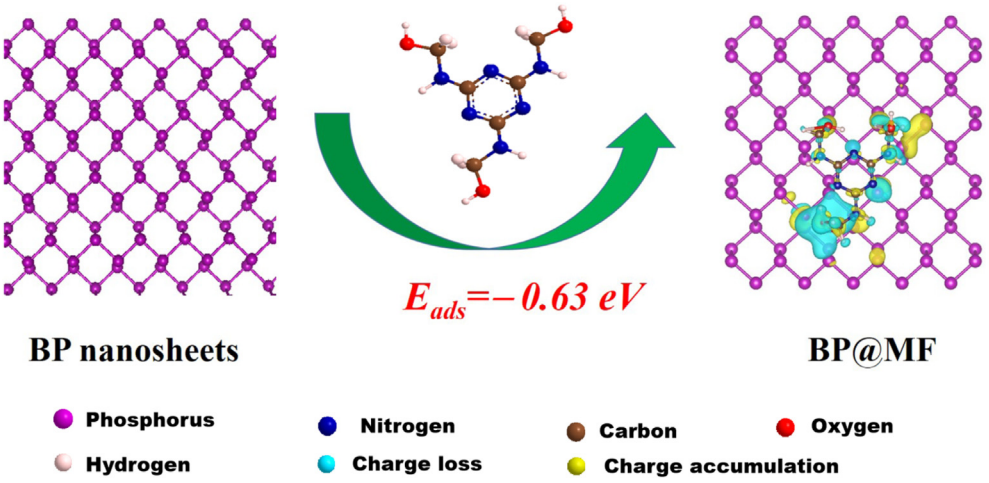

Fig. 2. Top view of adsorption structures of MF adsorbed single layer BP nanosheets.

3. Results and discussion

3.1. Theoretical calculation of feasibility for BP@MF

To verify the possibility of surface functionalization between BP nanosheets and MF, density functional theory (DFT) calculations [36] based on the first-principles [26] is employed to calculate the interaction between BP nanosheets and MF (details displays in the Table S1 and Fig. S1).

The adsorption energy is calculated by the following equation:

$$E_{ads} = E_{BP+mol} - E_{BP} - E_{mol} \quad (1)$$

where E_{BP}, E_{BP+mol} and E_{mol} is the total energy of phosphorene, the molecule adsorbed system and isolated molecule, respectively.

The most stable structures are shown in Fig. 2, which indicates that MF is located onto the supercell of 5 × 4 in BP layer with N and O being interlaced with P atoms. The adsorption energy is −0.63 eV from Eq. (1), which suggests there exists a strong mutual adsorption between BP nanosheets and MF. As a small molecule, MF resin can easily absorb on the surface of BP to compensate for the loss of van der Waals interactions between the phosphorene layers. The charge density is only distributed between the MF molecule and the BP layer, indicating a physisorption process, which is consist with Shao's work [36]. Under the shear forces originating from the stripping and mechanical stirring process, radicals and ions will be generated from the edge defect of BP layers and react with N to form P-N bonds as shown in Fig. 5 (e) and (f), which suggests there also exist a chemisorption [36]. The adsorption of MF on the surface of BP can prevent the contact of oxygen with phosphorene and enhance the compatibility of phosphorene with resin matrix.

3.2. Microstructure of BP and its functionalization

To reveal the morphology and structure of BP and BP@MF, a series of investigation and characterization is performed. The scanning electron microscope (SEM) is employed to observe the microscopic morphology of BP crystals, BP and BP@MF (Fig. 3a-c). Fig. 3(a) shows BP crystals have a typical multilayer structure with large size [31]. Fig. 3(b) shows the exfoliated BP has a thinner lamellar structure with a length of about fourteen micrometers, a width of about seven micrometers. For BP@MF, Fig. 3(c) reveals some white matter is connected around BP, and the surface of BP@MF is smoother than that of the exfoliated BP, which indicates BP nanosheets has been functionalized by MF resin. The size of BP becomes much smaller after functionalization, which is because that the adsorption of MF resin on the surface of BP may weaken the interaction of BP layers and thus favor the stripping, inhibiting its re-stacking and aiding the preparation of small BP nanosheets. The transmission electron microscope (TEM) is usually used to observe the internal fine structure of the sample. As shown in Fig. 3(d), the TEM image demonstrates few-layer BP is successfully stripped. Fig. 3(e) indicates the high-resolution TEM (HRTEM) image of BP, the lattice fringes of 0.33 nm and 0.53 nm are assigned to the (0 2 1) and (0 2 0) planes of BP [11,36], which is in line with the results of XRD tests. The selected-area electron diffraction pattern shows the exfoliated BP has a complete orthorhombic crystalline in Fig. 3(f). Fig. 3(g) exhibits a typical honeycomb structure of few layer phosphorus atom [1]. Few-layer BP is also testified by atomic force microscopy (AFM) image from Fig. 3(h) and (i). The AFM image presents BP have a relatively uniform surface with the average thickness of 1.23 nm and 0.95 nm. Generally, a monolayer phosphorene has a thickness of 0.53 nm [11,24,31,36]. Therefore, the thickness of 0.95 nm and 1.23 nm observed from Fig. 3(i) correspond to two to three layers of p atoms. These results are very consistent with the observations from Fig. 3(b) and (d), which demonstrates that the few-layers BP has been successfully fabricated.

The energy dispersive spectrometer (EDS) is employed to characterize the element distribution in the BP@MF nanosheets as shown in Fig. 4. Fig. 4(a) shows the SEM image of BP@MF nanosheets, indicating the small BP nanosheets is encapsulated in the MF resin. The element distribution diagrams from the selected area in Fig. 4(a) are displayed in Fig. 4(b)-(e), the content of nitrogen element exceeds 24 wt%, demonstrating BP is decorated with MF polymer. Meanwhile, the mapping images of carbon (Fig. 4(f)), nitrogen (Fig. 4(g)), oxygen (Fig. 4(h)) and phosphorus (Fig. 4(i)) further verify the successful formation of BP@MF nanosheets.

The X-ray diffraction (XRD) and Raman are also conducted to characterize the BP@MF, as shown in Fig. 5 (a) and (b). Several representative peaks located at 16.7°, 26.4°, 34.1°, 34.8°, 52.2°, 55.8° and 56.7° are ascribed to the (0 2 0), (0 2 1), (0 4 0), (1 1 1), (0 6 0), (1 5 1) and (0 6 1) interlayered planes of BP [24,31,37]. Compared to BP, these peaks also appear on the XRD of BP@MF, but the intensity of the peak is generally weakened, because of the MF resin covering on the surface of BP. The Raman spectra of BP exhibits three symbolic vibrational modes of BP, which are situated the peak of A_g^1 at about 361.2 cm^{-1}, B_{2g} at about 437.5 cm^{-1}, A_g^2 at about 466.2 cm^{-1} [17,24]. These peaks are also found in BP@MF sample, which demonstrates that the MF functionalization of BP does not change its original vibration structure. Compared to BP, a slight red shift (about 2 cm^{-1}) can be observed, which is attributed to the increased thickness of BP after encapsulated with MF polymer. To further clarify the interaction between BP and MF, X-ray photoelectron spectroscopy (XPS) is conducted to detect the chemical valence bond and composition of BP and BP@MF. Fig. 5 (c)

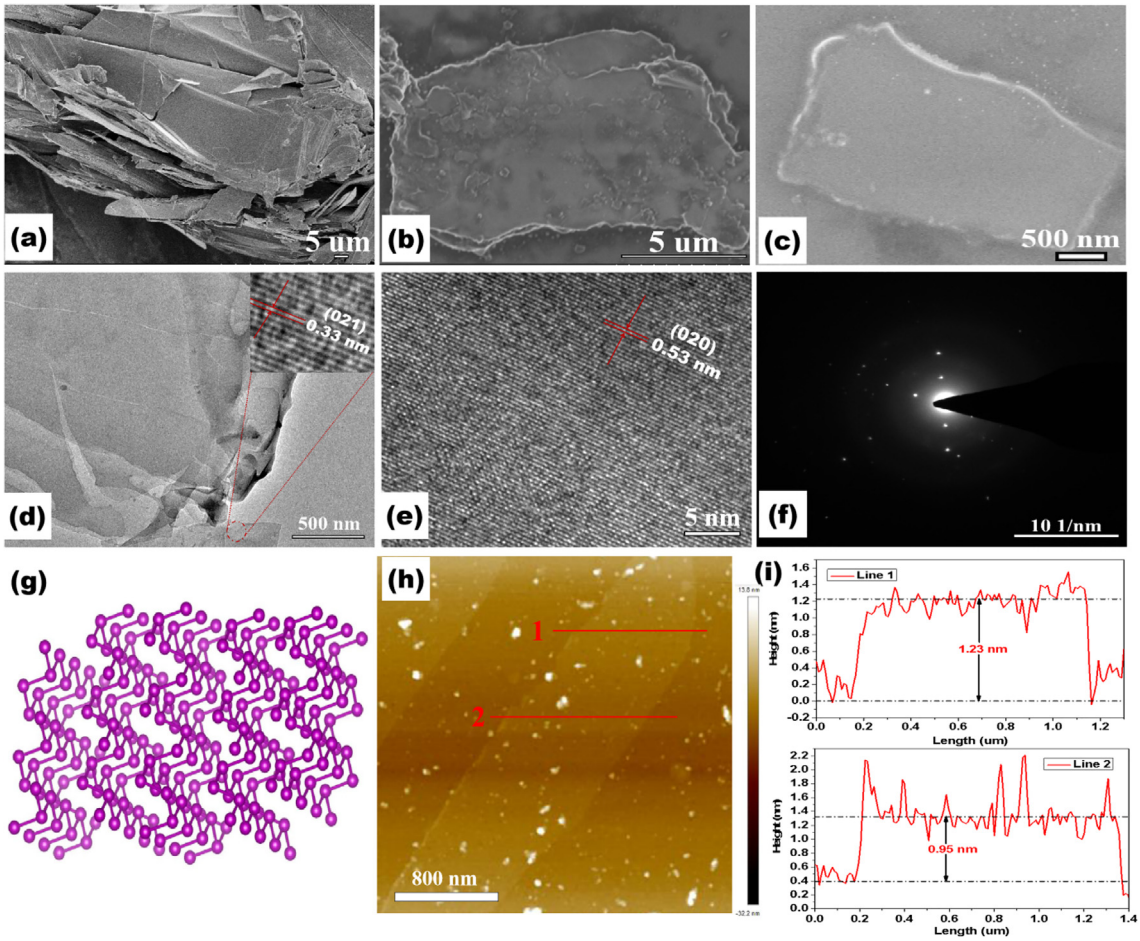

Fig. 3. SEM image: (a) BP crystal; (b) BP nanosheets; (c) BP@MF; (d) TEM image of BP nanosheets; (e) SAED pattern of BP nanosheets; (f) HRTEM image of BP nanosheets; (g) the atomic structure of few-layer BP nanosheets; (h) AFM image of BP nanosheets; (i) the corresponding height of line 1 and line 2.

shows the survey spectra of BP and BP@MF, compared to the spectrum of BP, the elements content of N, C in the spectra of BP@MF are increased. The N element of BP@MF increases by 35.54% and the atomic ratio of N/P increases from 0.04 (BP) to 26.34 (BP@MF) (Table S2), which indicates the BP is successfully functionalized by MF. As shown in Fig. 5(d), two peaks of BP located at binding energies of 129.7 and 130.5 eV matching to P $2P_{3/2}$ and P $2P_{1/2}$ signals, respectively [31,38]. The additional peak at 133.6 eV is ascribed to partial oxidation of BP [2,39]. BP is inevitably oxidized during the experiment process, this result has been verified from the O 1 s XPS of BP in Fig. 5(c). For BP@MF, its P 2P XPS spectrum is shown in Fig. 5(e). Four peaks centered at 129.6, 130.4, 133.0 and 134.0 eV are consistent with P-P bonds of P $2P_{3/2}$ and P $2P_{1/2}$ signals, P-N, and P-O bonds, respectively [12,36,40]. Compared to BP, the P $2P_{3/2}$ and P $2P_{1/2}$ peaks of BP@MF are moved to lower binding energies by about 0.1 eV, demonstrating a damage of long-range order and the oxidized phosphorus on the surface of BP@MF [36]. Notice that a P-N bond with the peak at 133.0 eV is detected from the P 2P XPS spectrum of BP@MF. This phenomenon is also testified by N 1S XPS spectrum in Fig. 5(f). Three peaks at 398.7, 399.9 and 405.7 eV are associated with N–H, C–N, and P–N bonds, respectively [31,36]. The Fourier transform infrared spectrometry (FTIR) is also conducted to investigate characteristic absorption peaks of BP and BP@MF. As shown in Fig. 5(g), compared to the several characteristic peaks of BP, some new peaks come out from BP@MF as follows, the peaks at 1561 and 1330 cm^{-1} correspond to the stretching vibration of C=N and the stretching vibration of C–N from MF resin, respectively [33]. The peak at 805 cm^{-1} is attributed to the stretching mode of P-N bond [41]. All the above evidences suggest BP is functionalized by MF polymer, revealing the edge of P atom react with N atom to form P-N bonds. Edge functionalization is very common in the decoration of 2D layered nanomaterials, such as $–NH_2$ functionalized ultrathin black phosphorene and –OH modified graphene nanosheets [12,42]. During the exfoliation process, radicals and ions can be produced from the edge of defective BP layers, which reacts with N atoms to form surface groups [36]. Thermogravimetric analysis (TGA) is employed to probe the mass loss process of BP and BP@MF under nitrogen. As shown from Fig. 5(h), BP has only one thermal decomposition stage, nevertheless, MF resin shows three-step mass loss from room temperature to 1000 °C. The degradation products in the first step are mainly water and melamine (about 20% mass loss). The second step occurs in the range of 350–450 °C, which is ascribed to the main decomposition of MF resin and the weight loss is about 80%. The third step occurs at above 650 °C corresponding to the further decomposition of char residues [43]. For BP@MF, it contains two main stages of thermal decomposition until 1000 °C. The first thermal degradation step appears between 250 and 400 °C, approaching to the thermal decomposition of MF. The second step takes place at 400 and 500 °C, due to the decomposition of BP. In Fig. 5(i), the derivative thermogravimetric analysis (DTG) indicates the maximum weight loss rates of BP and BP@MF are much lower than that of MF resin, which are attributed to the higher thermal stability of BP. The TGA curves (Fig. 5(h) shows BP has a residue of 45.06% at the temperature of 1000 °C and the residue of BP@MF is 27.43%, while MF resin has completely degraded. Therefore, the loading ratio of MF on BP is 1:4.67.

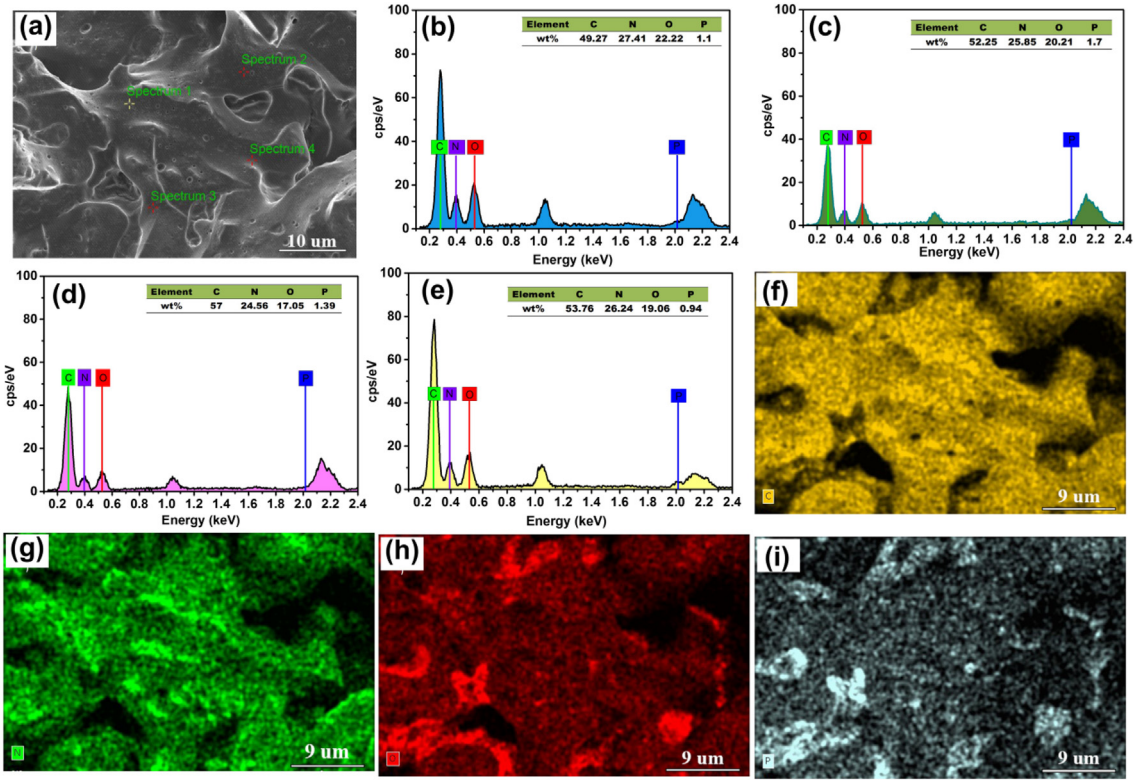

Fig. 4. EDS analysis of BP@MF: (a) SEM image of BP@MF nanosheets; (b) distribution diagram of element from Spectrum 1 in (a); (c) distribution diagram of element from Spectrum 2 in (a); (d) distribution diagram of element from Spectrum 3 in (a); (e) distribution diagram of element from Spectrum 4 in (a); mapping image: (f) carbon (C), (g) nitrogen (N), (h) oxygen (O), (i) phosphorus (P).

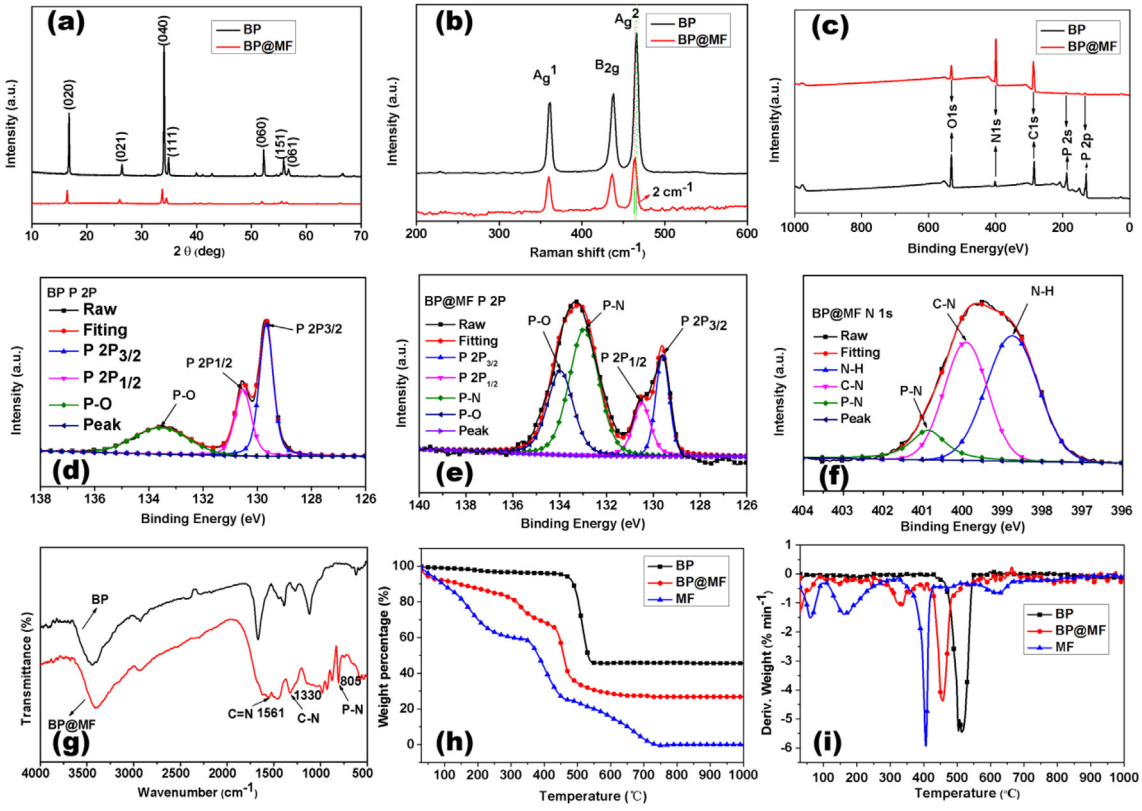

Fig. 5. Characterization of BP and BP@MF: (a) XRD patterns; (b) Raman spectra; (c) XPS survey spectra; (d) high-resolution P2p XPS spectra of BP; (e) high-resolution P2P XPS spectra of BP@MF; (f) high-resolution N1s XPS spectra of BP@MF; (g) FT-IR spectra of BP and BP@MF; (h) TGA curves of BP, BP@MF and MF; (i) DTG curves of BP, BP@MF and MF.

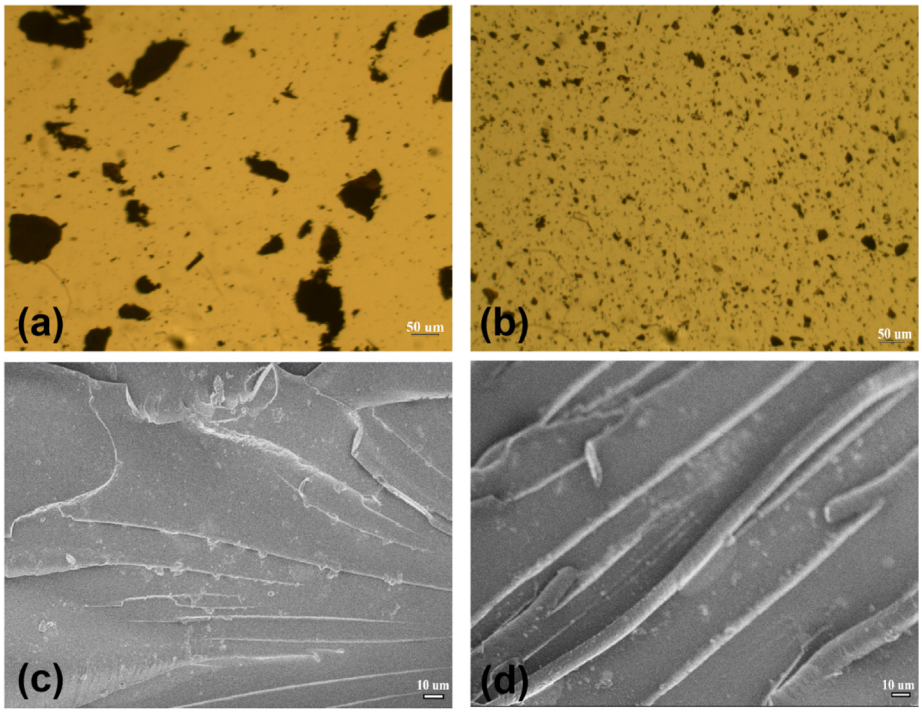

Fig. 6. The optical microscope images: (a) BP in EP matrix; (b) BP@MF in EP matrix; SEM image: (c) BP in EP matrix; (d) BP@MF in EP matrix.

3.3. Dispersibility of BP and BP@MF in epoxy resin

It is well known that the dispersion of nanofillers in polymer resins has an important influence on the mechanical properties and flame retardancy of polymer nanocomposites [44]. BP is a two-dimensional inorganic nanomaterial with poor dispersibility and interfacial compatibility in polymer matrix, which seriously undermines the comprehensive properties of polymer nanocomposites [31]. Therefore, it is of great significance to improve the dispersibility of BP in polymer resins. The dispersion of BP and BP@MF in EP resins is observed by the optical microscope images. Under the optical microscope, the dispersion of BP and BP@MF in EP matrix is more clearly and intuitively exhibited in Fig. 6(a) and (b). Obviously, BP is re-aggregated severely in EP resins with poor dispersion, while the EP nanocomposites with the addition of BP@MF has better dispersion than EP nanocomposites with the addition of BP. The same results can also be testified by SEM. The microscopic morphology of the freeze-fractured surface of EP/BP and EP/BP@MF nanocomposites are investigated in Fig. 6(c) and (d). Apparently, BP is massively stacked in the nanocomposites as shown in Fig. 6(c). Compared to EP/BP, BP@MF with uniform dispersion in EP matrix can be observed in Fig. 6(d), which indicates that the functionalization of BP with MF resin can significantly enhance the compatibility between nano-additive and resin matrix, thereby improves the dispersion of BP@MF in EP matrix.

3.4. Thermal stability of EP composites

TGA analysis is employed to evaluate the thermal property of EP/BP@MF nanocomposites, the detailed thermal degradation data are displayed in Table S3. Fig. 7(a) presents that EP/BP@MF nanocomposites has similar thermal degradation behavior as pure EP, which has a one-step weight loss process in the range of 300–500 °C. Compared to pure EP, with the increase of BP@MF and BP, there is a significant enhancement in carbon residue content at 800 °C. With increasing BP@MF content from 0.3 to 1.2 wt%, the char residues of EP/BP@MF nanocomposites are enhanced by 30.7–70.9%. However, for the EP/BP 1.2 sample, its char yield is only 17.36%, lower than char residue (19.40%) of EP/BP@MF 1.2, which indicates that the functionalization of BP by MF enhances the catalytic charring effect. In Fig. 7(b), the derivative thermogravimetric analysis (DTG) demonstrates the maximum weight loss rates of EP/BP nanosheets and EP/BP@MF nanocomposites are greatly lower than that of neat EP. This is because that the thermal stable structure of BP hinders the exchange of oxygen and the diffusion of flammable gases and MF can promote the char formation during the combustion, thereby improving the resistance of nanocomposites against thermal decomposition [31].

To study the influence of BP@MF on the thermomechanical properties of EP nanocomposites, the Dynamic Mechanical Analysis (DMA) is employed to test the storage modulus and tan δ of EP, EP/BP and EP/BP@MF composites. As shown in Fig. 7(c), the storage modulus of pure EP is 2430 M pa at room temperature, while the storage modulus value of EP/BP nanocomposites has dropped to 1970 M pa at the same temperature, with an 18.93% decrease compared to pure EP resin. This is because the direct addition of BP in the epoxy will cause a serious agglomeration, which causes a decrease in the storage modulus, the result is consistent with the image of the optical microscope. For EP/BP@MF nanocomposites, when the temperature is lower than 125 °C, as the amount of BP@MF increases from 0.3% to 1.2%, the storage modulus of EP/BP@MF nanocomposites increases by 2.06%, 4.94%, 9.47% and 13.99%, respectively. The increase of storage modulus is mainly due to the improved compatibility of BP@MF to epoxy resin. BP has a strong stiffness and thus has a certain enhancement to EP. The glass transition temperature (T_g) of EP nanocomposites can be indicated from the tan δ curves. In Fig. 7(d), with the addition of BP and BP@MF into EP matrix, all the tan δ peaks are slightly moved to lower temperature. The decrease of glass transition temperature may be due to the interface interaction of BP@MF affecting the crosslink density of the epoxy resin. On the other hand, it may be ascribed to the filling interface which is not very dense during the epoxy filling process, and the volume between the interfaces provides a certain free space for the segment movement [45].

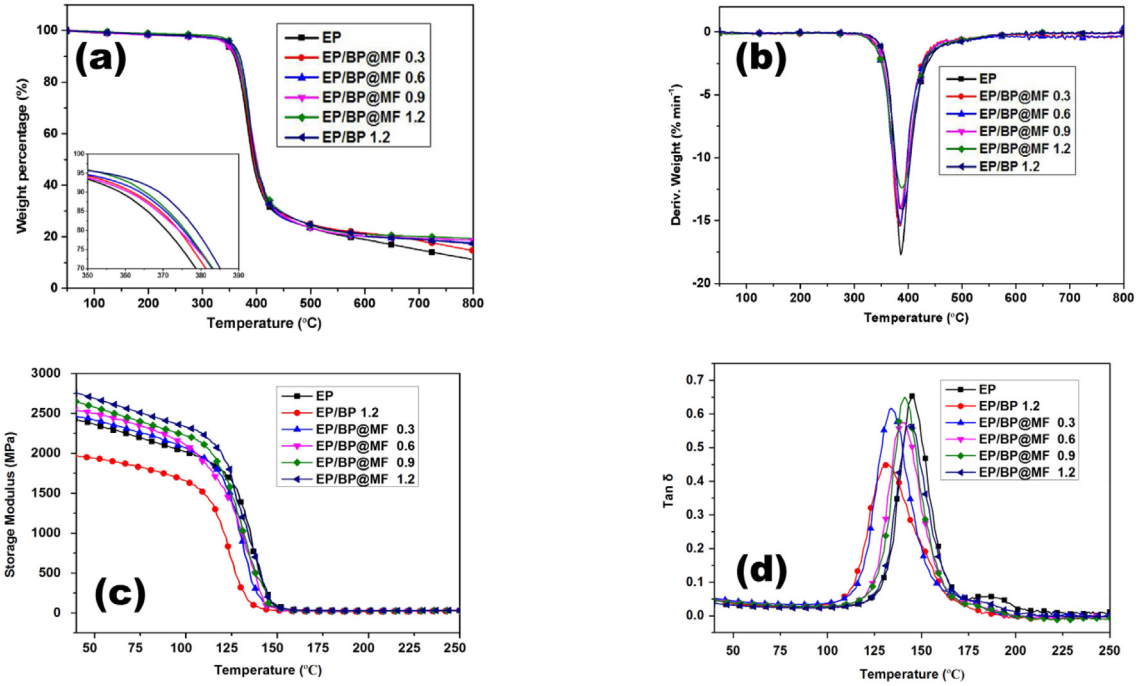

Fig. 7. (a) TGA curves and (b) DTG curves of EP and its nanocomposites with different addition of BP@MF; (c) storage modulus curves and (d) tan δ curves of EP and its nanocomposites with different addition of BP@MF.

3.5. Flame retardant properties of EP composites

The flame retardancy of EP nanocomposites are detected by microscale combustion calorimeter (MCC), UL-94 vertical burning tests and limiting oxygen index (LOI), which can fully evaluate the combustion of polymer nanocomposites [46,47]. The heat release rate (HRR) is always considered to be the most crucial parameter to assess the flame retardant [48–50]. Fig. 8(a) exhibits the HRR curves of pure EP and EP nanocomposites determined by MCC. As can be distinctly seen, the PHRR of pure EP reaches 1100 W g^{-1}, whereas adding only 1.2 wt% BP@MF, the PHRR of EP/BP@MF 1.2 nanocomposites decreases significantly to 623.7 W g^{-1}, which is reduced by 43.3% than that of pure EP. As a contrast, the HRR of EP/MF 1.2 and EP/BP 1.2 nanocomposites are also studied. The PHRR of EP/MF 1.2 and EP/BP 1.2 are lower than that of pure EP and higher than that of BP@MF 1.2, with a peak of 891.5 and 666.5 W g^{-1}, respectively. The total heat release (THR) is shown in Table S4. The THR of EP/BP@MF 1.2 nanocomposites (34.6 kJ g^{-1}) decreases by 12.6% than the THR of pure EP (39.6 kJ g^{-1}), while the THR of EP/MF 1.2 and EP/BP sheets is approached to pure EP, with a total heat release of 39.2 and 38.5 kJ g^{-1}. These results verify the fact that the introduction of BP@MF 1.2 in EP matrix effectively restricts the heat release rate of EP/BP@MF nanocomposites during combustion, implying the superior flame retardant properties of BP@MF. Moreover, the fire growth rate (FIGRA) is also employed to evaluate the fire hazard of the nanocomposites [51]. The FIGRA can be expressed as follows:

$$\text{FIGRA} = \frac{\text{PHRR}}{\text{tPHRR}} \tag{2}$$

Based on Table S4 and Equation (2), The FIGRA of pure EP is 3.35 W g^{-1} s^{-1}, whereas the FIGRA of EP/MF 1.2 and EP/BP 1.2 nanocomposite are 2.73 W g^{-1} s^{-1} and 2.16 W g^{-1} s^{-1}, respectively. Particularly, the FIGRA of EP/BP@MF 1.2 nanocomposites decreases by 41.2% (1.97 W g^{-1} s^{-1}) in contrast to that of pure EP, which manifests that the fire growth rate can be effectively reduced by the addition of BP@MF in EP polymer. The limiting oxygen index (LOI) and the UL-94 vertical burning tests of EP composites are shown in Fig. 8 (b). Pure EP burns easily with a lower LOI value of 24.7%, whereas the LOI value of

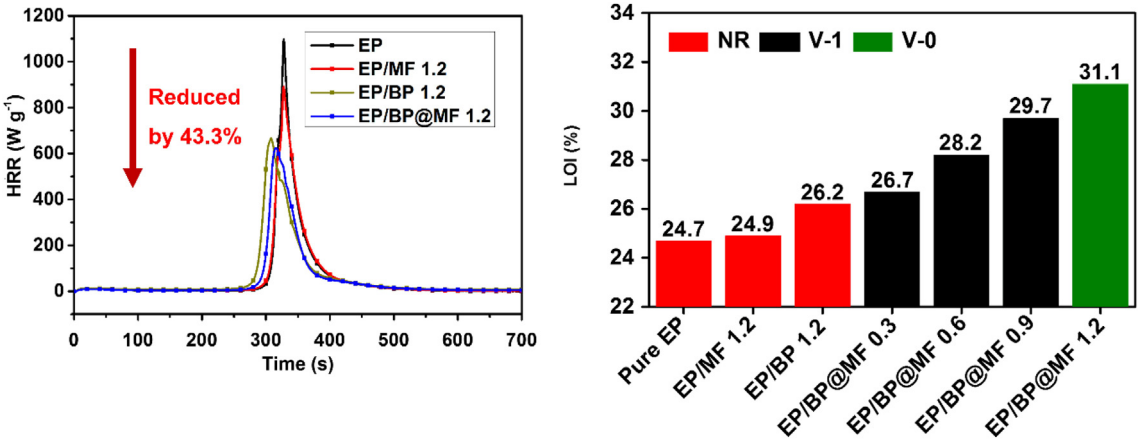

Fig. 8. (a) HRR versus time curves of EP and its nanocomposites; (b) LOI values and UL-94 vertical burning of EP and its nanocomposites.

ARTICLE IN PRESS

EP/BP@MF nanocomposites are dramatically improved by 8.1–25.9% with the introduction of BP@MF content from 0.3 to 1.2 wt%. Especially when BP@MF is incorporated into EP with the amount of 1.2 wt %, the LOI value reaches 31.1%. However, compared to EP/MF 1.2 and EP/BP 1.2 nanocomposites, the LOI value are only 24.9% and 26.2%, respectively. This result demonstrates that MF resin with very little addition in EP resin has little effect on the improvement of LOI value, and BP is easy to agglomerate, which also affects the improvement of LOI value. BP functionalized by MF resin can significantly improve the dispersibility of BP in EP matrix, and maximize the flame retardant effect of BP, thus improve the LOI value of EP nanocomposites. Unlike the LOI value testing, the UL-94 vertical burning tests can provide a more intuitive and objective evaluation for real combustion behavior. The pure EP and EP/MF 1.2 composite reveal no rating (NR), while by increasing BP@MF content from 0.3 to 0.9 wt%, the EP composites can easily reach V-1 rating. When the addition of BP@MF in EP matrix reaches 1.2 wt%, the EP/BP@MF nanocomposite can successfully pass V-0 flammability rating test. For EP/BP composite, the UL-94 vertical burning test displays no rating (NR). This is because that BP is easy to re-aggregate when directly adding it into the EP resin, which will have a negative influence on the flame retardancy. Whereas the BP functionalized by MF can be well dispersed in the EP matrix, which is beneficial to the retardation of fire during the combustion process [30]. Particularly note is that all the EP/BP@MF composites have no dripping phenomenon, reflecting the remarkable anti-dripping properties of BP@MF on epoxy resin. The detailed data can be seen in Table S5. After leaving the fire, the pure EP burnt intensely, while the EP/BP@MF 1.2 nanocomposite can self-extinguish at 3 s (Burning video in supporting information). It can be speculated that the incorporation of BP@MF promotes the formation of carbon residues with higher thermal stability, which can inhibit the transfer heat and enhance the flame retardant efficiency.

Filler efficiency is often used to characterize the contribution of a unit weight of filler to material properties [52]. The efficiency of the filler for PHRR is evaluated by its decline rate of per unit weight defined as $\phi_{PHRR} = \frac{PHRRm - PHRR}{PHRRm \times wt\%}$, where PHRR is peak heat release rate of the composite, PHRRm is peak heat release rate of the matrix material and wt% is the weight fraction of filler. Similarly, the ϕ_{LOI} is employed to characterize the efficiency of the filler for LOI, it can be defined as $\phi_{LOI} = \frac{LOI - LO\mathrm{Im}}{LO\mathrm{Im} \times wt\%}$, where LOI is limiting oxygen index of the composite, LOIm is limiting oxygen index of the matrix material and wt% is the weight fraction of filler. To better compare our work with previous researches, Table 1 summarizes previous report about the efficiency of the filler for flame retardant properties with various fillers. The data shows that the efficiency of the filler for ϕ_{PHRR} and ϕ_{LOI} in our EP/BP@MF composites is indeed extremely high, which indicates a higher flame retardant efficiency can be achieved by incorporating a smaller amount of BP @ MF into the epoxy matrix.

To observe the thermal degradation process of EP composites, the TG-FTIR technique is employed to investigate the volatile product emissions of EP, EP/BP, EP/BP@MF nanocomposites. Fig. 9 shows the absorbance intensities of the main pyrolysis products versus time relationship of different EP nanocomposites. Several representative peaks for the released gaseous products of EP nanocomposites are indicated as below:[31] the peak located at 2975 cm^{-1} is ascribed to the characteristic absorption of hydrocarbons and 2350 cm^{-1} is assigned to the characteristic absorption of carbon dioxide (CO_2); the peak located at 2150 cm^{-1} is ascribed to the characteristic absorption of carbon monoxide (CO) and the peak located at 1750 cm^{-1} is attributed to the characteristic absorption of carbonyl compounds; the peak located at 1510 cm^{-1} corresponds to the characteristic absorption of aromatic compounds. With the addition of 1.2 wt% of BP and BP@MF into EP, all the maximum absorbance intensities of main volatile products are obviously decreased compared to that of pure EP. Apparently, the addition of BP@MF 1.2 nanocomposites exhibits lowest absorbance intensity of all the main volatile products than that of EP/BP 1.2 and pure EP composites. This is because the addition of BP@MF 1.2 promotes the formation of char layer during combustion and reduces the release of volatile gases, which is in complete agreement with the TGA analysis. For CO_2, pure epoxy contains a large amount of C element, which inevitably generates a large amount of CO_2 during combustion. The direct addition of BP in the epoxy resin is easy to agglomerate, which cannot obtain a good flame retardant effect, so the amount of CO_2 will increases as the burning time increases. By adding BP@MF into the epoxy resin, a good flame retardant effect can be obtained. When the burning time is prolonged, the EP/BP@MF composite can extinguish, and thus the amount of CO_2 will decrease as the burning time is prolonged. CO is generally considered to be the main toxic gas in epoxy combustion. After more than 30 min, the CO absorption of EP/BP nanocomposites is slightly higher than that of pure EP, because BP is easily agglomerated in epoxy, resulting in insufficient combustion. However, for EP/BP@MF nanocomposites, its CO absorption decreases with time, indicating BP@MF isolates the contact of oxygen with the polymer, thereby effectively reducing the absorption of harmful gases. The reduction of volatile gases is beneficial to reduce the toxicity of smoke and heat release, thereby improving flame retardancy [41].

The char residues of EP nanocomposites formed from combustion can provide a perspective to explore the flame retardant mechanism. The SEM images of char layer for EP, EP/BP 1.2 and EP/BP@MF 1.2 composites are displayed in Fig. 10. For pure EP, the surface of the char residue is loose and contains some big opening hole (Fig. 10(a)). As a contrast, the char layer of EP/BP composites exhibits a very compact

Table 1
The Efficiency of the Filler for ϕ_{PHRR} and ϕ_{LOI} in Previous Literature.

Filler	Fraction (wt%)	ϕ_{PHRR}	ϕ_{LOI}	Matrix	Ref.
MCU-APP	30	1.74%	3.33%	PP	[43]
GO-CNF	20	1.25%	0.95%	Nanocellulose	[49]
CH/APP/CH/PAA-KAO	17.8	3.75%		PUF	[50]
PD-LDH@MF	15	4.60%	3.24%	EVA	[53]
MH-APP	13.7		3.37%	PU	[47]
PMMA–Ca_3Al	10	5.40%		Layered double hydroxide	[48]
FRs-rGO	5	7.00%	8.10%	Epoxy	[54]
Ionic liquid-based metal–organic hybrid	6	5.17%		Epoxy	[51]
g-C_3N_4/OAHPi hybrids	4	6.93%		PS	[9]
1-Vinyl-3-(diethoxyphosphoryl)-propylimidazolium bromide	4	16.25%	8.48%	Epoxy	[46]
BP/G	3.55	13.57%		WPU	[4]
FR@PZS	3	15.33%		Epoxy	[41]
BP-EC-Exf	3	14.83%		PUA	[30]
FRGO	2	21.50%		Epoxy	[6]
BP-PZN	2	29.70%		Epoxy	[31]
BP@MF	1.2	36.08%	21.06%	Epoxy	This work

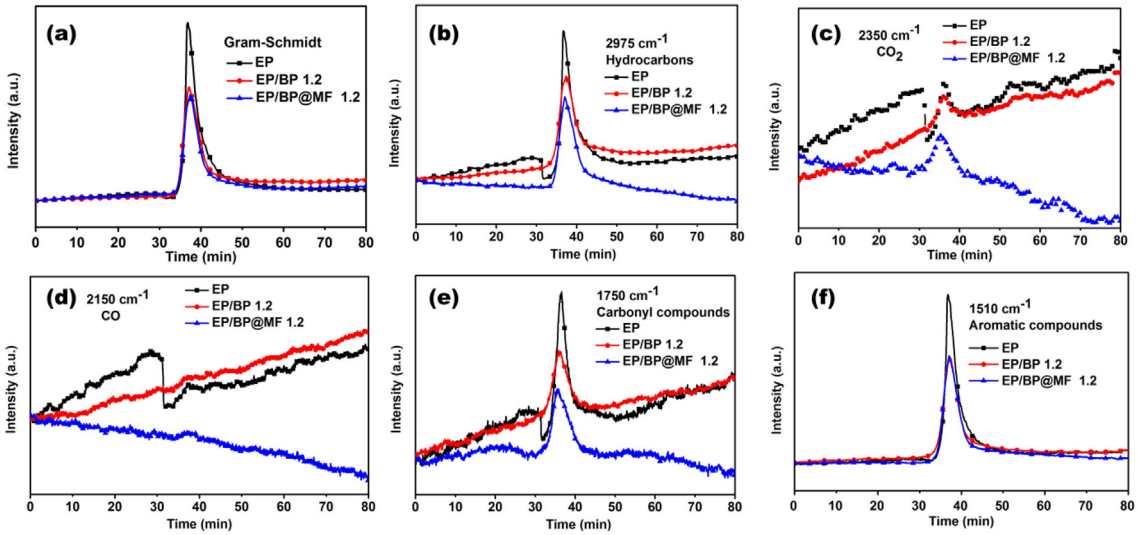

Fig. 9. Intensity of pyrolysis gas for EP, EP/BP 1.2 and EP/BP@MF 1.2 sample versus time: (a) total pyrolysis gases; (b) hydrocarbons; (c) CO_2; (d) CO; (e) carbonyl compounds; (f) aromatic compounds.

structure with a small amount of microspores (Fig. 10(b)). Meanwhile, Fig. 10(c) shows a more compact and condense structure with fewer holes on the surface of EP/BP@MF 1.2 nanocomposites, attributing to the BP and BP@MF can enhance the compactness of char layer in the combustion, which may be due to the isolation of oxygen from the polymer during burning process. As is well known, the formation of the char layer can protect the polymer from oxygen and heat, hinder the transfer of heat and release of flammable products, thereby achieving the safety of fire [46]. Therefore, it can be speculated that the addition of BP and BP@MF are beneficial to promote the formation of carbon layer, and thus improving the flame retardancy of the composite.

The carbonization degree is an effective evaluation index for combustion products, the degree of carbonization is higher, and it is more favorable to prevent the material burning. Raman spectroscopy is conducted to evaluate the ingredient and structure of char layer. The Raman spectra of EP and its nanocomposites is shown in Fig. 10(d)-(f). Two representative peaks located at 1375 cm^{-1} and 1585 cm^{-1} are identified as D peak and G peak, respectively. In previous works, the statistical area ratio of D peak to G peak (ID/IG) can be utilized to measure the carbonization degree and a lower I_D/I_G value is meant to a higher graphitization degree. Obviously, the I_D/I_G value of neat EP is 5.12 (Fig. 10(d)), while the EP/BP 1.2 nanocomposite exhibits an I_D/I_G value of 3.96 (Fig. 10(e)), the EP/BP@MF 1.2 nanocomposite reveals a lower I_D/I_G value of 3.43 (Fig. 10(f)), demonstrating the high carbonization can be obtained with the introduction of BP@MF into EP matrix, which is ascribed to the catalytic charring effect of MF functionalized BP in EP combustion.

The FT-IR spectra is also conducted to analyze the char residues of EP and EP/BP@MF nanocomposites. In Fig. 11(a), the peaks at 1600, 1510, 1440, 1240, 1127, 825 and 622 cm^{-1} are associated with carbonized aromatic structure, which can be discovered in EP and EP nanocomposites. Compared to pure EP, the char residues of EP/BP and EP/BP@MF nanocomposites show a weak peak at 1370 and 1171 cm^{-1}, which are attributed to the stretching modes of P═O and P–O–P structures [4]. Besides, EP/BP@MF nanocomposites also exhibit an absorption peak at 827 cm^{-1}, responding to the typical absorption of

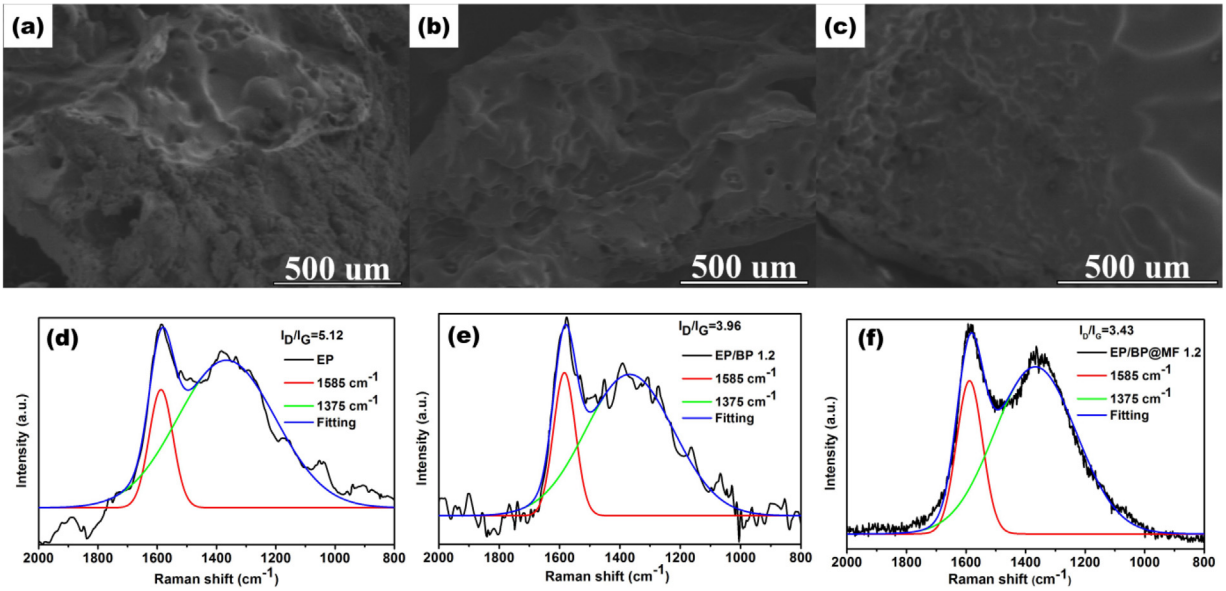

Fig. 10. SEM image of char residues: (a) pure EP; (b) EP/BP 1.2 nanocomposites; (c) EP/BP@MF 1.2 nanocomposites; Raman spectra of char residues: (d) pure EP; (e) EP/BP 1.2 nanocomposites; (f) EP/BP@MF 1.2 nanocomposites.

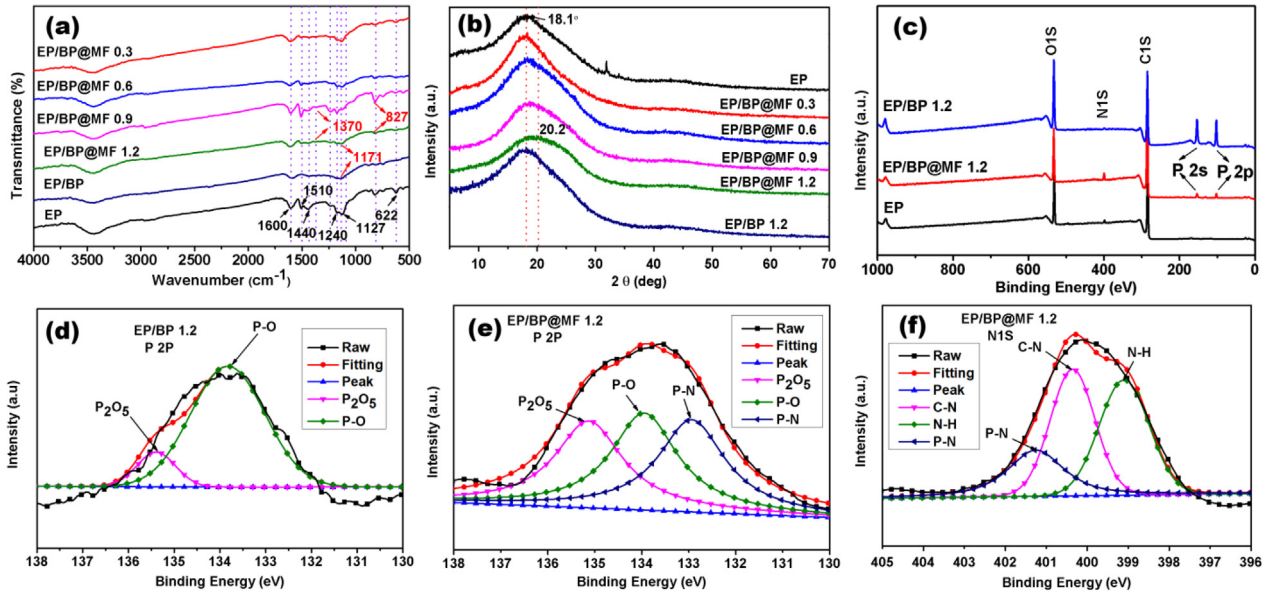

Fig. 11. (a) FT-IR spectra and (b) XRD patterns for char residues of pure EP and its nanocomposites; (c) XPS survey spectra of the char residues for pure EP, EP/BP 1.2 and EP/BP@MF 1.2 nanocomposites; high-resolution P2p XPS spectra: (d) EP/BP 1.2; (e) EP/BP@MF 1.2; (f) high-resolution N1s XPS spectra of EP/BP@MF 1.2.

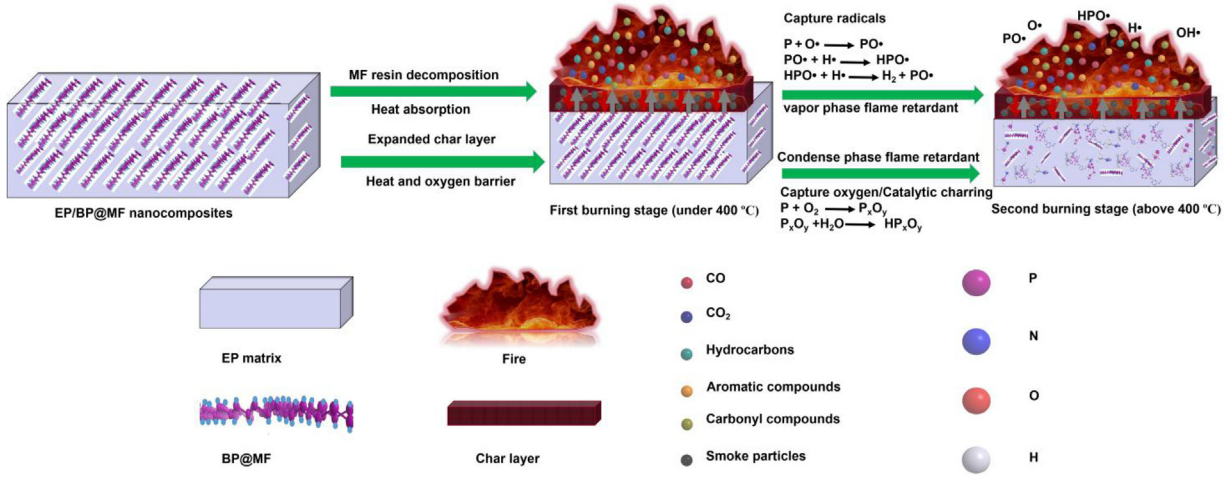

Fig. 12. Illustration of flame retardant mechanism for BP@MF in EP matrix.

P-N bonds, demonstrating the formation of P-N bonds between BP and MF resin. The XRD patterns of the char layer for EP and its nanocomposites are shown in Fig. 11(b). There appears a wide diffraction peak at 18.1°, with an inter-planar spacing of 0.4895 nm, demonstrating the formation of expanded graphitized carbon compared to the inter-planar spacing of graphite. For EP/BP@MF 1.2, there exists a wide peak at 20.2°, with an inter-planar spacing of 0.4380 nm, revealing the introduction of BP@MF is conducive to the formation of a dense char layer, the result is very consistent with the SEM of char layer in Fig. 10. Meanwhile there is no peak ascribed to BP, indicating the BP and BP@MF in EP matrix are fully degraded in the combustion process, the results can also be testified by the proposal mechanism in Fig. 12. XPS analysis can provide some detailed information about element composition and structure of the char residues. Fig. 11(c) shows the XPS survey spectra of pure EP, EP/BP and EP/BP@MF nanocomposites, their surfaces all contain the elements of C, N and O, the P element only exists in the char residues of EP/BP 1.2 and EP/BP@MF 1.2 nanocomposites, due to the formation of P_xO_y in the combustion of BP-containing polymer [55]. The XPS spectra in P2p region for EP/BP 1.2 and EP/BP@MF 1.2 nanocomposites are shown in Fig. 11(d) and (e). Fig. 11(d) exhibits the P2p peaks for EP/BP 1.2 can be separated into two peaks at 134.0 eV and 135.5 eV, which is attributed to P–O and P_2O_5 bonds, respectively [31]. Fig. 11(e) shows the P2p peaks for EP/BP@MF 1.2 can be separated into three peaks at 133.0, 134.0 and 135.5 eV, which is assigned to P–N, P–O and P_2O_5 bonds, respectively, indicating the formation of P_xO_y and P–N bonds [31]. The same proof can be obtained from the N1s XPS spectra of EP/BP@MF 1.2 in Fig. 11(f), there are three peaks, which can be ascribed to N–H, C–N and P–N bonds, respectively. These results are fully consistent with the XPS spectra of BP@MF in Fig. 5(e) and (f), proving once again that BP has been successfully functionalized by MF resin.

3.6. Flame retardant mechanism

Based on the above results and analysis for combustion behavior in EP/BP@MF 1.2 nanocomposites, a possible flame retardation mechanism is proposed in Fig. 12. The flame inhibition process can be divided into two main stages. In the first stage, when the temperature is lower than 400 °C, the melamine–formaldehyde resin is heated and sublimated to absorb heat, which will lower the temperature of the polymer matrix and delay the heat transfer [56]. Meanwhile, the edge of BP functionalized by the MF will form a phosphorus-nitrogen

compound, which forms expanded char layers during thermal pyrolysis, acting as a thermal and oxygen barrier layer, indicating a condensed phase flame retardant mechanism. In the second stage, when the temperature is higher than 400 °C, the BP which does not participate in the functionalization starts to thermally decompose. According to the previous reports [30,31], the decomposition of BP is very similar to that of red phosphorus. On the one hand, BP may form various active radicals (PO_2·, PO·, and HPO·) during combustion, scavenging H· and OH· radicals to reduce the generation of flammable gases (Fig. 9) and acting as a vapor phase flame retardant mechanism [57]. On the one hand, BP is mainly oxidized into P_xO_y [26,28], the P_xO_y reacts with water formed by pyrolysis of polymers to produce various types of phosphoric acid derivatives. These phosphoric acid derivatives promote the formation of char layers (Fig. 7(a) and Fig. 10), produce more stable P═O and P–O–P structures (Fig. 11(a)), and isolate oxygen and heat transfer (The PHRR and THRR are decreased as shown in Fig. 8(a)), achieving the mechanism of condense phase flame retardant.

4. Conclusion

In this work, few-layer BP nanosheets is exfoliated and then decorated by MF resin via surface functionalization. The results of calculations and experiments demonstrates that MF resin has been successful in adsorbing onto the BP surface. The surface decoration by forming the P-N bonds dramatically solves the aggregation phenomenon and improves the dispersibility of BP in EP matrix. The resultant BP@MF is incorporated into EP to prepare EP/BP@MF nanocomposites. Addition of 1.2 wt% BP@MF into EP exhibits excellent thermal stability and mechanical properties. In addition, the PHRR and THRR values of EP/BP@MF nanocomposites are significantly decreased and its LOI value is dramatically improved. TG-FTIR analysis demonstrates that all the intensities of pyrolysis products are significantly inhibited with the introduction of BP@MF. Characterization of char residues indicates that BP@MF is beneficial to the formation of a dense char layer. A two-step flame retardant mechanism is proposed for the vapor and condensed phase products in combustion. A facile, low addition and economical method for superior flame retardancy and surface functionalization of BP nanosheets is accomplished in the study, and the functionalization strategy will promote the application of BP-polymer-based nanocomposites.

Declaration of Competing Interest

The authors declare that they have no known competing financial interests or personal relationships that could have appeared to influence the work reported in this paper.

Acknowledgements

This work was supported by National Key R&D Program of China (2017YFD0601003) and Science and Technology Planning Project of Guangzhou (201804010174).

Appendix A. Supplementary data

Supplementary data to this article can be found online at https://doi.org/10.1016/j.cej.2019.122991.

References

[1] H. Liu, Y. Du, Y. Deng, P.D. Ye, Semiconducting black phosphorus: synthesis, transport properties and electronic applications, Chem. Soc. Rev. 44 (2015) 2732–2743.
[2] A. Favron, E. Gaufres, F. Fossard, A.L. Phaneuf-L'Heureux, N.Y. Tang, P.L. Levesque, A. Loiseau, R. Leonelli, S. Francoeur, R. Martel, Photooxidation and quantum confinement effects in exfoliated black phosphorus, Nat. Mater. 14 (2015) 826–832.
[3] J. Pang, A. Bachmatiuk, Y. Yin, B. Trzebicka, L. Zhao, L. Fu, R.G. Mendes, T. Gemming, Z. Liu, M.H. Rummeli, Applications of phosphorene and black phosphorus in energy conversion and storage devices, Adv. Energy Mater. 8 (2018).
[4] X. Ren, Y. Mei, P. Lian, D. Xie, W. Deng, Y. Wen, Y. Luo, Fabrication and application of black phosphorene/graphene composite material as a flame retardant, Polymers (Basel) 11 (2019).
[5] J.-H. Choi, P. Cui, W. Chen, J.-H. Cho, Z. Zhang, Atomistic mechanisms of van der Waals epitaxy and property optimization of layered materials, Wiley Interdiscip. Rev.: Comput. Mol. Sci. 7 (2017).
[6] B. Yu, Y. Shi, B. Yuan, S. Qiu, W. Xing, W. Hu, L. Song, S. Lo, Y. Hu, Enhanced thermal and flame retardant properties of flame-retardant-wrapped graphene/epoxy resin nanocomposites, J. Mater. Chem. A 3 (2015) 8034–8044.
[7] W. Wu, L. Wang, R. Yu, Y. Liu, S.H. Wei, J. Hone, Z.L. Wang, Piezophototronic effect in single-atomic-layer MoS2 for strain-gated flexible optoelectronics, Adv. Mater. 28 (2016) 8463–8468.
[8] R. Arenal, A. Lopez-Bezanilla, Boron nitride materials: an overview from 0D to 3D (nano)structures, Wiley Interdiscip. Rev.: Comput. Mol. Sci. 5 (2015) 299–309.
[9] Y. Shi, B. Yu, L. Duan, Z. Gui, B. Wang, Y. Hu, R.K.K. Yuen, Graphitic carbon nitride/phosphorus-rich aluminum phosphinates hybrids as smoke suppressants and flame retardants for polystyrene, J. Hazard. Mater. 332 (2017) 87–96.
[10] Y. Shi, C. Liu, L. Liu, L. Fu, B. Yu, Y. Lv, F. Yang, P. Song, Strengthening, toughing and thermally stable ultra-thin MXene nanosheets/polypropylene nanocomposites via nanoconfinement, Chem. Eng. J. 378 (2019).
[11] Y. Zhang, X. Rui, Y. Tang, Y. Liu, J. Wei, S. Chen, W.R. Leow, W. Li, Y. Liu, J. Deng, B. Ma, Q. Yan, X. Chen, Wet-chemical processing of phosphorus composite nanosheets for high-rate and high-capacity lithium-ion batteries, Adv. Energy Mater. 6 (2016).
[12] X. Zhu, T. Zhang, Z. Sun, H. Chen, J. Guan, X. Chen, H. Ji, P. Du, S. Yang, Black phosphorus revisited: a missing metal-free elemental photocatalyst for visible light hydrogen evolution, Adv. Mater. 29 (2017).
[13] X. Ren, P. Lian, D. Xie, Y. Yang, Y. Mei, X. Huang, Z. Wang, X. Yin, Properties, preparation and application of black phosphorus/phosphorene for energy storage: a review, J. Mater. Sci. 52 (2017) 10364–10386.
[14] M.J. Nine, M.A. Cole, D.N.H. Tran, D. Losic, Graphene: a multipurpose material for protective coatings, J. Mater. Chem. A 3 (2015) 12580–12602.
[15] H. Guo, Y. Li, J. Zheng, J. Gan, L. Liang, K. Wu, M. Lu, Reinforcement in the mechanical properties of shape memory liquid crystalline epoxy composites, J. Appl. Polym. Sci. 132 (2015) n/a-n/a.
[16] Y. Mu, M.S. Si, The mechanical exfoliation mechanism of black phosphorus to phosphorene: a first-principles study, EPL (Europhys. Lett.) 112 (2015).
[17] D. Hanlon, C. Backes, E. Doherty, C.S. Cucinotta, N.C. Berner, C. Boland, K. Lee, A. Harvey, P. Lynch, Z. Gholamvand, S. Zhang, K. Wang, G. Moynihan, A. Pokle, Q.M. Ramasse, N. McEvoy, W.J. Blau, J. Wang, G. Abellan, F. Hauke, A. Hirsch, S. Sanvito, D.D. O'Regan, G.S. Duesberg, V. Nicolosi, J.N. Coleman, Liquid exfoliation of solvent-stabilized few-layer black phosphorus for applications beyond electronics, Nat. Commun. 6 (2015) 8563.
[18] Z. Luo, G. Qi, K. Chen, M. Zou, L. Yuwen, X. Zhang, W. Huang, L. Wang, Microwave-assisted preparation of white fluorescent graphene quantum dots as a novel phosphor for enhanced white-light-emitting diodes, Adv. Funct. Mater. 26 (2016) 2739–2744.
[19] J.R. Brent, N. Savjani, E.A. Lewis, S.J. Haigh, D.J. Lewis, P. O'Brien, Production of few-layer phosphorene by liquid exfoliation of black phosphorus, Chem. Commun. (Camb.) 50 (2014) 13338–13341.
[20] Z. Shen, S. Sun, W. Wang, J. Liu, Z. Liu, J.C. Yu, A black–red phosphorus heterostructure for efficient visible-light-driven photocatalysis, J. Mater. Chem. A 3 (2015) 3285–3288.
[21] J. Sun, G. Zheng, H.W. Lee, N. Liu, H. Wang, H. Yao, W. Yang, Y. Cui, Formation of stable phosphorus-carbon bond for enhanced performance in black phosphorus nanoparticle-graphite composite battery anodes, Nano Lett. 14 (2014) 4573–4580.
[22] P. Yasaei, B. Kumar, T. Foroozan, C. Wang, M. Asadi, D. Tuschel, J.E. Indacochea, R.F. Klie, A. Salehi-Khojin, High-quality black phosphorus atomic layers by liquid-phase exfoliation, Adv. Mater. 27 (2015) 1887–1892.
[23] M. Lee, A.K. Roy, S. Jo, Y. Choi, A. Chae, B. Kim, S.Y. Park, I. In, Exfoliation of black phosphorus in ionic liquids, Nanotechnology 28 (2017) 125603.
[24] Y. Zhao, H. Wang, H. Huang, Q. Xiao, Y. Xu, Z. Guo, H. Xie, J. Shao, Z. Sun, W. Han, X.F. Yu, P. Li, P.K. Chu, Surface coordination of black phosphorus for robust air and water stability, Angew. Chem. Int. Ed. Engl. 55 (2016) 5003–5007.
[25] L. Zhang, L.-F. Gao, L. Li, C.-X. Hu, Q.-Q. Yang, Z.-Y. Zhu, R. Peng, Q. Wang, Y. Peng, J. Jin, H.-L. Zhang, Negatively charged 2D black phosphorus for highly efficient covalent functionalization, Mater. Chem. Front. 2 (2018) 1700–1706.
[26] H. Hu, H. Gao, L. Gao, F. Li, N. Xu, X. Long, Y. Hu, J. Jin, J. Ma, Covalent functionalization of black phosphorus nanoflakes by carbon free radicals for durable air and water stability, Nanoscale 10 (2018) 5834–5839.
[27] G. Abellan, V. Lloret, U. Mundloch, M. Marcia, C. Neiss, A. Gorling, M. Varela, F. Hauke, A. Hirsch, Noncovalent functionalization of black phosphorus, Angew. Chem.-Int. Ed. 55 (2016) 14557–14562.
[28] L. Wu, J. Wang, J. Lu, D. Liu, N. Yang, H. Huang, P.K. Chu, X.F. Yu, Lanthanide-coordinated black phosphorus, Small (2018) e1801405.
[29] X. Ren, Y. Mei, P. Lian, D. Xie, Y. Yang, Y. Wang, Z. Wang, A novel application of phosphorene as a flame retardant, Polymers (Basel) 10 (2018).
[30] S. Qiu, B. Zou, H. Sheng, W. Guo, J. Wang, Y. Zhao, W. Wang, R.K.K. Yuen, Y. Kan, Y. Hu, Electrochemically exfoliated functionalized black phosphorene and its polyurethane acrylate nanocomposites: synthesis and applications, ACS Appl. Mater. Interfaces 11 (2019) 13652–13664.
[31] S. Qiu, Y. Zhou, X. Zhou, T. Zhang, C. Wang, R.K.K. Yuen, W. Hu, Y. Hu, Air-stable polyphosphazene-functionalized few-layer black phosphorene for flame retardancy of epoxy resins, Small 15 (2019) e1805175.

ARTICLE IN PRESS

[32] Y. Wu, H. Zhang, A. Pan, Q. Wang, Y. Zhang, G. Zhou, L. He, White-light-emitting melamine-formaldehyde microspheres through polymer-mediated aggregation and encapsulation of graphene quantum dots, Adv. Sci. (Weinh) 6 (2019) 1801432.
[33] F. Luo, K. Wu, X. Huang, W. Hu, M. Lu, Encapsulation of graphite nanoflakes for improving thermal conductivity of mesogenic epoxy composites, Ind. Eng. Chem. Res. 56 (2017) 489–494.
[34] A. Hu, H. Peng, M. Li, S. Fu, Preparation of melamine-formaldehyde encapsulated fluorescent dye dispersion and its application to cotton fabric printing, Color. Technol. 135 (2018) 103–110.
[35] X. Wang, P. Wu, Melamine foam-supported 3D interconnected boron nitride nanosheets network encapsulated in epoxy to achieve significant thermal conductivity enhancement at an ultralow filler loading, Chem. Eng. J. 348 (2018) 723–731.
[36] L. Shao, H. Sun, L. Miao, X. Chen, M. Han, J. Sun, S. Liu, L. Li, F. Cheng, J. Chen, Facile preparation of NH2-functionalized black phosphorene for the electrocatalytic hydrogen evolution reaction, J. Mater. Chem. A 6 (2018) 2494–2499.
[37] J. Wang, D. Liu, H. Huang, N. Yang, B. Yu, M. Wen, X. Wang, P.K. Chu, X.F. Yu, In-plane black phosphorus/dicobalt phosphide heterostructure for efficient electrocatalysis, Angew. Chem. Int. Ed. Engl. 57 (2018) 2600–2604.
[38] W. Lei, T. Zhang, P. Liu, J.A. Rodriguez, G. Liu, M. Liu, Bandgap- and local field-dependent photoactivity of Ag/black phosphorus nanohybrids, ACS Catal. 6 (2016) 8009–8020.
[39] E.A. Lewis, J.R. Brent, B. Derby, S.J. Haigh, D.J. Lewis, Solution processing of two-dimensional black phosphorus, Chem. Commun. 53 (2017) 1445–1458.
[40] M.T. Edmonds, A. Tadich, A. Carvalho, A. Ziletti, K.M. O'Donnell, S.P. Koenig, D.F. Coker, B. Ozyilmaz, A.H. Neto, M.S. Fuhrer, Creating a stable oxide at the surface of black phosphorus, ACS Appl. Mater. Interfaces 7 (2015) 14557–14562.
[41] S. Qiu, X. Wang, B. Yu, X. Feng, X. Mu, R.K.K. Yuen, Y. Hu, Flame-retardant-wrapped polyphosphazene nanotubes: a novel strategy for enhancing the flame retardancy and smoke toxicity suppression of epoxy resins, J. Hazard. Mater. 325 (2017) 327–339.
[42] C. Liu, X. Liu, J. Tan, Q. Wang, H. Wen, C. Zhang, Nitrogen-doped graphene by all-solid-state ball-milling graphite with urea as a high-power lithium ion battery anode, J. Power Sources 342 (2017) 157–164.
[43] K. Wu, Z. Wang, Y. Hu, Microencapsulated ammonium polyphosphate with urea-melamine-formaldehyde shell: preparation, characterization, and its flame retardance in polypropylene, Polym. Adv. Technol. 19 (2008) 1118–1125.
[44] X. Wang, W. Xing, X. Feng, L. Song, Y. Hu, MoS2/polymer nanocomposites: preparation, properties, and applications, Polym. Rev. 57 (2017) 440–466.
[45] F. Luo, K. Wu, H. Guo, Q. Zhao, M. Lu, Anisotropic thermal conductivity and flame retardancy of nanocomposite based on mesogenic epoxy and reduced graphene oxide bulk, Compos. Sci. Technol. 132 (2016) 1–8.
[46] F. Xiao, K. Wu, F. Luo, Y. Guo, S. Zhang, X. Du, Q. Zhu, M. Lu, An efficient phosphonate-based ionic liquid on flame retardancy and mechanical property of epoxy resin, J. Mater. Sci. 52 (2017) 13992–14003.
[47] F. Luo, K. Wu, Y. Li, J. Zheng, H. Guo, M. Lu, Reactive flame retardant with core-shell structure and its flame retardancy in rigid polyurethane foam, J. Appl. Polym. Sci. 132 (2015) n/a-n/a.
[48] Y. Gao, J. Wu, Q. Wang, C.A. Wilkie, D. O'Hare, Flame retardant polymer/layered double hydroxide nanocomposites, J. Mater. Chem. A 2 (2014).
[49] B. Wicklein, A. Kocjan, G. Salazar-Alvarez, F. Carosio, G. Camino, M. Antonietti, L. Bergstrom, Thermally insulating and fire-retardant lightweight anisotropic foams based on nanocellulose and graphene oxide, Nat. Nanotechnol. 10 (2015) 277–283.
[50] X. Liu, S. Qin, H. Li, J. Sun, X. Gu, S. Zhang, J.C. Grunlan, Combination intumescent and kaolin-filled multilayer nanocoatings that reduce polyurethane flammability, Macromol. Mater. Eng. 304 (2018).
[51] F. Xiao, K. Wu, F. Luo, S. Yao, M. Lv, H. Zou, M. Lu, Influence of ionic liquid-based metal-organic hybrid on thermal degradation, flame retardancy, and smoke suppression properties of epoxy resin composites, J. Mater. Sci. 53 (2018) 10135–10146.
[52] K.M. Shahil, A.A. Balandin, Graphene-multilayer graphene nanocomposites as highly efficient thermal interface materials, Nano Lett. 12 (2012) 861–867.
[53] J.-Z. Du, L. Jin, H.-Y. Zeng, B. Feng, S. Xu, E.-G. Zhou, X.-K. Shi, L. Liu, X. Hu, Facile preparation of an efficient flame retardant and its application in ethylene vinyl acetate, Appl. Clay Sci. 168 (2019) 96–105.
[54] X. Qian, L. Song, B. Yu, B. Wang, B. Yuan, Y. Shi, Y. Hu, R.K.K. Yuen, Novel organic–inorganic flame retardants containing exfoliated graphene: preparation and their performance on the flame retardancy of epoxy resins, J. Mater. Chem. A 1 (2013).
[55] T. Zhang, Y. Wan, H. Xie, Y. Mu, P. Du, D. Wang, X. Wu, H. Ji, L. Wan, Degradation chemistry and stabilization of exfoliated few-layer black phosphorus in water, J. Am. Chem. Soc. 140 (2018) 7561–7567.
[56] K. Wu, Z.Z. Wang, Intumescent flame retardation of EVA using microencapsulated ammonium polyphosphate and pentaerythritols, Polym.-Plast. Technol. Eng. 47 (2008) 247–254.
[57] L.L. Xu, L.H. Xiao, P. Jia, K. Goossens, P. Liu, H. Li, C.G. Cheng, Y. Huang, C.W. Bielawski, J.X. Geng, Lightweight and ultrastrong polymer foams with unusually superior flame retardancy, ACS Appl. Mater. Interfaces 9 (2017) 26392–26399.